An early modern human presence in Sumatra at 73-63 kyr

Authors: Westaway, K.E.[1], Louys, J.[2], Due Awe, R.*[3], Morwood, M.J.*[4], Price, G.J.[5], Zhao, J.-x.[5], Aubert, M. [6], Joannes-Boyau, R.[7], Smith, T.M.[8,9], Skinner, M.M.[10,11], Compton, T.[12], Bailey, R.M. [13], van den Bergh, G.D.[4], de Vos, J.[14], Pike, A.W.G[15], Stringer, C.[12], Saptomo, E.W.[3], Rizal,Y.[16], Zaim, J.[16], Santoso, W.D.[16], Trihascaryo, A.[16], Kinsley, L.[17], Sulistyanto, B.[3]

Author affiliations:

[1]Department of Environmental Sciences, Faculty of Science and Engineering, Macquarie University, NSW 2109
[2]School of Culture, History, and Languages, ANU College of Asia and the Pacific, Australian National University, Canberra, Australia.
[3]Indonesian Centre for Archaeology, Jl. Raya Condet Pejaten No. 4, Jakarta 12001, Indonesia.
[4] Centre for Archaeological Sciences, School of Earth and Environmental Sciences, University of Wollongong, Wollongong, NSW 2522, Australia
[5]School of Earth and Environmental Sciences, University of Queensland, Brisbane, Qld 4072, Australia.
[6]Place, Evolution and Rock Art Heritage Unit (PERAHU), Griffith University, Gold Coast, Queensland 4222, Australia
[7] Southern Cross GeoScience, Southern Cross University, Military Rd, Lismore, NSW, 2480.
[8] Australian Research Centre for Human Evolution, Environmental Futures Research Institute, Griffith University, 170 Kessels Road, Nathan, QLD 4111, Australia
[9] Department of Human Evolutionary Biology, Harvard University, 11 Divinity Avenue, Cambridge, MA 02138, USA.
[10] School of Anthropology and Conservation, University of Kent, Canterbury, CT2 7NR, UK
[11] Department of Human Evolution, Max Planck Institute for Evolutionary Anthropology, Deutscher Platz 6, 04103, Germany
[12] Department of Earth Sciences, Natural History Museum, Cromwell Road, London SW7 5BD, UK
[13]School of Geography and the Environment, University of Oxford, Oxford, OX12JD, UK
[14]Department of Geology, Naturalis Biodiversity Center, Leiden, The Netherlands
[15]Department of Archaeology, University of Southampton, Highfield Road, Southampton, SO17 1BF, UK.
[16] Geology Study Program, Institut Teknologi Bandung, Indonesia
[17] Research School of Earth Sciences, Australian National University, Canberra, Australia

**deceased*

Corresponding author: Dr Kira E. Westaway
Department of Environmental Sciences, Faculty of Science and Engineering, Macquarie University, NSW 2109
Email: kira.westaway@mq.edu.au
Tel: +62 9850 8429
Fax: +62 9850 8420

Keywords: Sumatra, geochronology, cave breccia, faunal turnover, human dispersal, palaeoenvironmental change

Running title: Age of the Lida Ajer human remains

Manuscript information: 3 figures

Word and character counts: 250 referenced paragraph, 1694 words in the text (including referenced paragraph but not including acknowledgements, references, and figure captions).

Genetic evidence for anatomically modern humans (AMH) out of Africa prior to 75 kyr[1] and in Island Southeast Asia (ISEA) before 60 kyr (93-61 kyr)[2] predates accepted archaeological records of occupation in the region[3]. Claims that AMH arrived in ISEA before 60 kyr[4] have only been supported by equivocal[5] or non-skeletal evidence[6]. AMH evidence from this period is rare and lacks robust chronologies due to a lack of direct dating applications[7], poor preservation and/or excavation strategies[8], and questionable taxonomic identifications[9]. Lida Ajer is a Sumatran Pleistocene cave with a rich rainforest fauna associated with fossil human teeth[10,7]. The significance of the site is unclear due to unsupported taxonomic identification of these fossils and uncertainties regarding the age of the deposit, thus is rarely considered in models of human dispersal. Here, we reinvestigate Lida Ajer to securely identify the teeth and establish a robust chronology using an integrated dating approach. Using enamel-dentine junction morphology, enamel thickness, and comparative morphology, we show that the teeth are unequivocally AMH. Luminescence and uranium-series techniques applied to bone-bearing sediments and speleothems, and coupled uranium-series and electron spin resonance dating of mammalian teeth place modern humans in Sumatra between 73-63 kyr. This age is consistent with biostratigraphic estimations[7], palaeoclimate and sea-level reconstructions, and genetic evidence for a pre-60 kyr arrival of AMH into ISEA[2]. Lida Ajer represents the earliest evidence of rainforest occupation by AMH, and underscores the importance of reassessing the timing and environmental context of the modern human dispersals out of Africa.

Lida Ajer is a small multi-chambered cave in the Padang Highlands situated to the south of Payakumbuh village, West Sumatra (Fig. 1 and Extended Data Fig. 1). A rear chamber (Fig. 1c), was excavated by Dubois between 1887-1890[10], which contains a rich fossiliferous breccia (Fig. 2) that preserves a rainforest fauna[11,7] (Extended Data Fig. 2). Two hominin teeth recovered from the deposit, an upper central incisor and second molar (Fig. 3D 1-2 and Extended Data Fig. 3), were classified as human based on their size and morphology[12]. Despite the potential significance of these finds, the age of the site is unconfirmed due to an estimated age of 90-60 kyr on the basis of biochronology[11] and relative age of >81 kyr using amino acid racemization (AAR) on bone[13,14].

Lida Ajer is one of a group of sites referred to as the Sumatran or Padang Caves. They also include Sibrambang and Djamboe[11] (both dated at >70 kyr by AAR on bone[14]) in addition to numerous unnamed caves excavated by Dubois in the Padang Highlands. Large numbers of orangutan fossils and other closed forest taxa have been recovered from these sites (Supplementary Table 2 and Extended Data Fig. 2), indicative of widespread humid rainforest environments in west Sumatra during the late Pleistocene[11,12,15]. Due to many similarities, the Sumatran faunas are considered coeval with Punung from East Java (128-118 kyr[16])[11,15]. The cave faunas from Sumatra and Java are considered intermediate in age between Ngandong and Wadjak (dated to 558-126 kyr[17] and 37-29 kyr[18], respectively, Extended Data Fig. 1b and Supplementary Table 1) and may date to penultimate interglacial period (~130-80 kyr)[11].

The fossil chamber in Lida Ajer comprises four areas of lithified deposits (Fig. 2). Each area consists of cemented breccias outcropping at the same topographic level, with large, allogenic angular clasts and fossils buried in a clay-rich matrix, overlain and underlain by flowstones. The individual deposits most likely represent the remains of a single, thick sedimentary unit that has since partially eroded, the maximum height of which is represented by the base of the calcite columns in Area 3 (Fig. 2B). The majority of species recovered in recent fieldwork (Extended Data Fig. 2) were also recorded by Dubois (Supplementary Table 2), although no additional hominin remains or archaeology were observed in the cave.

The Lida Ajer teeth are smaller than fossil orangutans and East and Southeast Asian *H. erectus* / archaic *H. sapiens* (Extended Data Fig. 3). They show greater affinity to East Asian Late Pleistocene *H. sapiens* than to Southeast Asian Late Pleistocene to mid Holocene *H. sapiens* (Supplementary Tables 3-4). The relative enamel thickness (RET) of the incisor is most similar to mean values for modern humans, and exceeds the extant orangutan range (Supplementary Table 5 and Extended Data Fig. 4). Molar RET is intermediate between mean values of living humans and living and fossil orangutans. Discriminant function analysis of molar enamel-dentine junction (EDJ) morphology classifies it as *H. sapiens* (Extended Data Figs 4-6). Both teeth have a simple external morphology typical of *H. sapiens*. They lack traits that characterise East and Southeast Asian *H. erectus* / archaic *H. sapiens* and *H. floresiensis*. Furthermore, derived *H. sapiens* features are found in both teeth, such as incisor double shovelling (SI sections 2-3). The combination of their small size and external and internal morphology demonstrates that they are anatomically modern *Homo sapiens*.

We employed a multidisciplinary dating approach to determine the age of the breccia. Red thermoluminescence (red TL) and post-infrared infrared-stimulated luminescence (pIR-IRSL) dating of the sediments provided burial ages, while U-series dating of associated speleothems yielded bracketing ages (Fig. 2). Several fossil teeth of *Pongo* and Siamang gibbon were also directly dated using a combination of U-series profiling and coupled U-series/ESR (US/ESR) dating. Those samples included new fossils recovered during our excavations, as well a specimen collected by Dubois[10] (Extended Data Fig. 8d). The resulting age estimates (Supplementary Tables 7, 8, 11) have been summarised in a composite stratigraphic figure (Fig. 3B, C). Technical considerations associated with dating the breccia matrix, fossil teeth and calcite are discussed in the Supplementary Information sections 4-7.

Maximum ages for the deposition of the breccia are constrained by ^{230}Th ages of a basal flowstone of 203 ± 17 kyr (LA-F3) and a straw stalactite dated to 84 ± 1 kyr (LA-08-29) that was recovered from the breccia itself. Straw stalactites with large diameters and thin walls (as in this study) precipitate, detach and drop into underlying sediment over relatively short timescales, and thus commonly represent ages close to the true time of sedimentary deposition[19]. A minimum age of the fossil breccia is constrained by ^{230}Th ages of overlying flowstones of 71 ± 7 kyr (LA-F1) and 11 ± 2 kyr (LA-F2). Thus, U-series dating of bracketing speleothems suggests that deposition of the fossils occurred between 84 ± 1 to 71 ± 7 kyr. Luminescence dating of the breccia supports this chronology with red TL suggesting that the quartz grains were last exposed to daylight 85 ± 25 kyr (maximum age), while single-aliquot dating of feldspars using pIR-IRSL yielded an age of 62 ± 5 kyr (which likely lies closer to the true age for breccia deposition[20]; Supplementary Table 7 and Extended Data Fig. 7). Direct dating of fossils yielded minimum ^{230}Th ages of >80-75 kyr (7,12,13,21/LA/5/08 – with Dubois's tooth 9967A ~70-60 kyr see SI) (Extended Data Fig. 8) and coupled US/ESR ages of 76 ± 7 kyr and 86 ± 13 kyr (12 and 13-LA-5-08 Extended Data Fig. 9). The results from each independent dating method are in stratigraphic agreement (Fig. 3B).

All chronological data were modelled in a modified Bayesian framework designed to take into account the minimum/maximum range, true age or burial age limitations of each age estimate. This provides the best estimate for the burial age and the first numerical age for the Lida Ajer fauna of 68 ± 5 kyr (1σ; age range 73-63 kyr) (Fig. 3c and Extended Data Fig. 10). This is broadly in agreement with the previous AAR estimations[14], regional biostratigraphic correlations[11] and regional sea-level reconstructions[21] enabling the appearance of a modern rainforest community in Sumatra during a period of connection to other Sunda landmasses.

The presence of modern humans in Sumatra between 73-63 kyr is significantly older (~20 kyr e.g.,[22]) than previous skeletal records in ISEA, but is consistent with new evidence for a human presence in

northern Laos 70-46 kyr[23], with genetics-based estimates of AMH presence in Asia prior to the Younger Toba Eruption[3] (although recent recalibration places it at 71.6 kyr[24]), and with stone tool evidence from Asia[25.] This minimum arrival date also agrees with mtDNA prediction of AMH in Southeast Asia at 79-75 kyr[2]. While it is at odds with popular estimates of an MIS 4 exit from Africa[3], it supports more recent lines of evidence that argue for an earlier exit from Africa[26].

The presence of a closed canopy rainforest ecosystem in Sumatra at 73-63 kyr is supported by pre-Toba pollen evidence from off-shore north Sumatra[27] as well as broad-scale palaeoenvironmental reconstructions of Pleistocene rainforest persistence in western Sumatra[15,28] (Fig. 1A). Significantly, our results provide the earliest unambiguous evidence of occupation of rainforest conditions by AMH. The longstanding preferred route of modern humans out of Africa has been along a 'coastal dispersal corridor'[29], which is thought to have occurred during MIS 4 when many Asian environments were considered inhospitable to early AMH. Marine environments offer particularly favourable conditions for human subsistence and movement. Conversely, rainforests, with their highly spaced, seasonal resources, scarce fat-rich faunas, and dearth of carbohydrate-rich plants[30], present serious difficulties for movement and colonisation by hominins that evolved in open environments. Successful exploitation of rainforest environments requires the capacity for complex planning and technological innovations: the behavioural hallmark of our species. Our data indicate that such innovations and capacities were in place in Asia well before MIS4. Furthermore, the presence of modern humans in the Padang Highlands indicates that humans were able to disperse beyond the coast when or shortly after arriving in Southeast Asia.

This new chronology for modern human arrival in Indonesia supports calls for a reassessment of the timing and environmental context of human movement out of Africa. An age of 73-63 kyr is consistent with mtDNA predictions[2] and emerging palaeoanthropological data from the broader region[23]. Our study provides unique insights into the chronological and environmental framework of dispersals through the region. Most significantly, we suggest that behavioural flexibility and technological innovations required for successful utilisation of complex and challenging environments, as seen in other caves in the region[22], were in place by the beginning of MIS4. Such traits were no doubt instrumental in precipitating the successful migration of modern humans out of Africa.

Online Content Methods, along with any additional Extended Data display items and Source Data, are available in the online version of the paper; references unique to these sections appear only in the online paper.

References

1. Pagani, L., Lawson, D.J., Jagoda, E., Mörseburg, A., Eriksson, A., Mitt, M., Clemente, F. *et al*., Genomic analyses inform on migration events during the peopling of Eurasia. *Nature* **538**, 238-242 (2016).

2. Fu, Q., Mittnik, A., Johnson, PL.F., Bos, K., Lari, M., Bollongino, R., Sun, C., Giemsch, L., Schmitz, R., Burger, J., Ronchitelli, AM, Martini, Cremonesi, R.G., Svoboda, J., Bauer, P., Caramelli, D., Castellano, S., Reich, D., Pa¨a¨bo S. & Krause J. A. Revised Timescale for Human Evolution based on Ancient Mitochondrial Genomes. *Current Biology* **23**, 553-559 (2013).

3. Oppenheimer, S. The great arc of dispersal of modern humans: Africa to Australia. *Quatern. Int.* **202**, 2–13 (2009).

4. Dennell, R. & Petraglia, M.D. The dispersal of *Homo sapiens* across southern Asia: how early, how often, how complex? *Quaternary Sci. Rev.* **47**, 15-22 (2012).

5 Liu, W., Martino´n-Torres, M.a., Cai, Y.-j., Song Xing, Tong, H.-w., Pei, S.-w., Sier, M.J., Wu, X.-h., Edwards, R.L., Cheng, H., Yi-yuan Li, Yang, X.-x., Castro, J.M, & Wu, X.-j. The earliest unequivocally modern humans in southern China. *Nature* **526**, 696–699 (2015).

6. Morwood M.J., Sutikna T., Saptomo E.W., Westaway, K.E., Jatmiko, Due Awe R., Moore M., Yuniawati D.Y., Hadi P., Zhao J.-x, Turney C.S.M., Fifield K., Allen H., & Soejono, R.P. Climate, people and faunal succession on Java, Indonesia: evidence from Song Gupuh. *J. Archaeol. Sci.* **35**, 1776-1789 (2008).

7. de Vos, J. *Mid-Pleistocene of Southern Asia*. *In:* The Encyclopedia of Quaternary Science (ed. Elias, S.A.) 3232-3249. (Elsevier, Oxford, 2007).
8. Morwood, M. J., Sutikna, T., Saptomo, E. W., Jatmiko, & Westaway, K. E. Preface: research at Liang Bua, Flores, Indonesia. *J. Hum. Evol.* **57,** 437–449 (2009).
9. Schwartz, J.H., Long, V.T., Cuong,N.L., Kha, L.T. Tattersall, I. A review of the Pleistocene hominoid fauna of the Socialist Republic of Vietnam (excluding Hylobatidae) *Anthropology Papers of the American Museum of Natural History*, **76**, 1–24 (1995).
10. Dubois, E. Voorloopig bericht omtrent het onderzoek naar de Pleistocene en tertiaire Vertebraten-Fauna van Sumatra en Java, gedurende het jaar 1890. *Natuurk. Tijdschr. Ned. Ind.* **51**, 93-100 (1891).
11. de Vos, J. The *Pongo* faunas from Java and Sumatra and their significance for biostratigraphical and paleo-ecological interpretations. *Proceedings of the Koninklijke Nederlandse Akademie van Wetenschappen Series B* **86**, 417-425 (1983).
12. Hooijer, D., A. Prehistoric teeth of man and of the orang-utan from central Sumatra, with notes on the fossil orang-utan from Java and Southern China. *Zool. Meded*. **29,** 175-301 (1948).
13. Skelton, R. *Aspartic acid racemisation dating of Southeast Asian sites*. Unpublished report (1985).
14. Drawhorn, G. M. *The Systematics and Paleodemography of Fossil Orangutans*. (PhD Thesis, University of California) 1–232 (Davis, 1994).
15. Louys, J., & Meijaard, E. Palaeoecology of Southeast Asian megafauna-bearing sites from the Pleistocene and a review of environmental changes in the region. *J. Biogeogr.* **37**, 1432-1449 (2010).
16. Westaway, K. E., Morwood, M. J., Roberts, R. G., Rokus, A. D., Zhao, J.-x., Storm, P., Aziz, F., van den Bergh, G. D., Hadi, P., Jatmiko, & de Vos, J. Age and biostratigraphic significance of the Punung rainforest fauna, East Java, Indonesia; implications for *Pongo* and *Homo*. *J. Hum. Evol.* **53**, 709-717 (2007).
17. Indriati, E., Swisher, C. C., Lepre, C., Quinn, R.L., Suriyanto, R.A., Hascaryo, A.T., Grün, R., Feibel, C.S., Pobiner, B.L., Aubert, M., Lees, W., & Antón, S.C. The age of the 20 meter Solo River Terrace, Java, Indonesia and the survival of *Homo erectus* in Asia. *PLoS One* **6**, 1-10 (2011).
18. Storm, P., Wood, R., Stringer, C., Bartsiokas, A., de Vos, J., Aubert, M., Kinsley, M., & Grün, R. U-series and radiocarbon analyses of human and faunal remains from Wajak, Indonesia. *J. Hum. Evol.* **64**, 356-365 (2013).
19. St Pierre, E., Westaway, K.E., Zhao, J-x., Gagan, M.K., Lentfer, C., Rokus Awe Due, Morwood, M.J., Hantoro, W.S., Djubiantono, T. & Suwargadi, B.W. Preliminary U-series and TL dating of deposits in Liang Bua sub-chamber, Flores, Indonesia. *J. Archaeol. Sci.* **40**, 148-155 (2013).
20. Roberts, R.G., Westaway, K.E., Zhao, J.-x., Turney, C.S.M., Rink, W.J., Bird, M.I., & Fifield, K. Geochronology of cave deposits in Liang Bua and river terraces in the Wae Racang valley, western Flores, Indonesia. *J. Hum. Evol.* **57,** 484-502 (2009).
21. Louys, J., & Turner, A. Environment, preferred habitats and potential refugia for Pleistocene *Homo* in Southeast Asia. *Comptes Rendus Palevol* **11**, 203-211 (2012).
22. Barker, G. & Farr, L. (eds.) *Archaeological investigations in the Niah Caves, Sarawak, 1954-2004*.: McDonald Institute for Archaeological Research ISBN 9781902937601 (McDonald Institute Monographs 2, Cambridge, 2016).
23. Shackelford, L., Demeter, F., Westaway, K.E., Duringer, P., Bacon, A-M., Ponche, J.L., Sayavongkhamdy, T., Zhao, J.-x., Barnes, L., Boyon, M., Sichanthongtip, P., Sénégas, Karpoff, A-M., Patole-Edoumba, E., Coppens, Y. & Braga, J. More evidences for early modern human morphological diversity in Southeast Asia at Tam Pa Ling, Laos. *Quatern. Int.* in press (accepted 7 December, 2016) https://doi.org/10.1016 /j.quaint.2016.12.002
24. Oppenheimer, S. A single southern exit of modern humans from Africa: Before or after Toba? *Quat. Int.* **258,** 88-99 (2012).
25. Petraglia, M.D., Ditchfield, P., Jones, S., Korisettar, R., & Pal, J.N. The Toba volcanic super-eruption, environmental change, and hominin occupation history in India over the last 140,000 years. *Quat. Int.* **258**, 119-134 (2012).
26. Groucutt, HS., Petraglia, MD, Bailey, G., Scerri, EMJ, Parton, A, Clark-Balzan, L, Jennings, RP, Lewis, L Blinkhorn, J., Drake, NA, Breeze, PS, Inglis, RH, Devès, MH, Meredith-Williams, M, Boivin, N, Thomas, MG. & Scally, A. Rethinking the Dispersal of *Homo sapiens* out of Africa. *Evol. Anthropol.* **24**, 149–164 (2015).
27. van der Kaars, S., Williams, M.A.J., Bassinot, F., Guichard, F., Moreno, E., Dewilde, F., & Cook, E.J. The influence of the ~73 ka Toba super-eruption on the ecosystems of northern Sumatra as recorded in marine core BAR94-25. *Quatern. Int.* **258**, 45-53 (2012).
28. Newsome, J. & Flense, J. R. Late Quaternary vegetational history of the Central Highlands of Sumatra. II. Palaeopalynology and vegetational history. *J. Biogeogr.* **15,** 555-578 (1988).
29 Erlandson, JM., Braje & TJ., 2015. Coasting out of Africa: The potential of mangrove forests and marine habitats to facilitate human coastal expansion via the Southern Dispersal Route. *Quatern. Int.* **382**, 31-41 (2015).
30. Roberts, P, & Petraglia, M. Pleistocene rainforests: barriers or attractive environments for early human foragers? *World Archaeol* **47**, 718-739 (2015).

Supplementary Information is linked to the online version of the paper at www.nature.com/nature.

Acknowledgements
This research was funded by Australian Research Council Discovery grants (DP1093049, DP140100919 and DP120101752) to KW, RJB, and GJP *et al*., respectively, and a Leaky Foundation grant and Research School of Asia and the Pacific Grant Development Support grant to JL. Chris Stringer's research is supported by the Human Origins Research Fund and the Calleva Foundation. We acknowledge the Max Planck Society for funding micro-CT scanning of the teeth, Anthony Olejnicak and JP Zermeno for assistance with section preparation, and support provided by the Centre from Archaeology in Padang Sumatra and ARKENAS in Jakarta and for allowing access to the site and four fossil faunal teeth for dating. We thank the Department of Geology, Naturalis Biodiversity Center, in Leiden, The Netherlands for providing access to Dubois's fieldnote book, excavation details, the two modern human teeth for scanning and the *Pongo* tooth for dating, and we thank Christopher Bronk Ramsey, for assistance with age modelling.

Author Contributions
KEW, RDA, JL, GJP, WDS mapped and excavated the site and collected faunal and dating samples, KEW conducted the red TL and pIR-IRSL dating, J-x.Z and GJP conducted the U-series measurements on the speleothem while MA and LK conducted U-series profiling on the fossil teeth and RJ-B conducted the US/ESR dating. GvdB and RDA analysed the fauna and MJM, GvdB, JdV, YR, JZ, WDS and AT helped to find and organise access to the site. TMS and JdV conducted the micro-CT scanning of the teeth, and TMS measured enamel thickness. TC and CS described the teeth and MMS analysed the EDJ. RMB aided in the design of the dating approach and conducted the Bayesian modelling, while AWGP conducted the modelling of the U-series age estimates. Finally, EWS and BS helped with the dating of the fauna and KEW, JL, GJP, JxZ, RJ-B, GvdB, MA, TMS, TC, MMS, CS and JdV, wrote the paper, with early contributions from MJM and RDA.

Author Information Reprints and permissions information is available at www.nature.com/reprints. The authors declare no competing financial interests. Readers are welcome to comment on the online version of the paper. Correspondence and requests for materials should be addressed to K.E.W. (kira.westaway@mq.edu.au).

Figure legends

Figure 1: Location of Indonesia, Sumatra, and Lida Ajer cave and associated breccia. **a**, Southeast Asia illustrating the location of Sumatra (redrawn with permission from[7]). **b**, Sumatra island illustrating the location of Lida Ajer, close to the volcanic Bukit Barisan Mountains, in belt of Carboniferous limestone. **c**, Cave plan and profile of Lida Ajer with its three chambers – Front, Bat and Fossil chambers and the four sampling locations. The fossil bearing breccia unit has been marked in brown with associated speleothem (flowstones, stalagmites and stalagmites) marked in grey. The sampling locations – Areas 1-4 are indicated on the plan and marked 1-4 in white circles on the profile.

Figure 2: Lida Ajer breccia; structure and stratigraphic relationships**. a**, An enlargement of the fossil chamber in Figure 1c (dashed box) demonstrating the stratigraphic relationships and sampling locations collected for U-series dating on the flowstones (rectangles) and soda straw (star), U-series and coupled US/ESR on the fossil teeth (hexagon), and red TL and pIR-IRSL on the breccia matrix (circle). **b**, The four main areas of breccia in the cave depicted by photographs. Areas 1-4 correlate with the marked sampling areas in **a,** and the symbols refer to the dating techniques listed in the key. **c,** The breccia from Area 1 showing the angular clasts and sandy clay matrix. **d**, The underlying

flowstone from Area 2 sampled for U-series dating (LA-F3). **e**, The calcite column from Area 3 sampled for U-series dating (LA-F2). **f**, The overlying flowstone from Area 4 sampled for U-series dating (LA-F1).

Figure 3: A summary of the results from the Lida Ajer cave analysis. **a**, The associated evidence 1-2) The human teeth from Lida Ajer discovered by Dubois and first identified by Hooijer (see Extended Data Figure 3 e-f for the full version); 3 – the soda straw stalactite discovered in the cave breccia and used for dating; 4-5) *Pongo sp.* fossil molar teeth used for U-series and coupled US/ESR dating (13 and 12/LA/5/08) (Extended Data Figs 8-9). **b**, A composite stratigraphy of the cave to simplify the stratigraphic relationships and associations with the fossil material. **c**, The new chronology for Lida Ajer using multiple dating techniques (red TL, U-series TIMS, U-series MC-ICPMS profiling and coupled US/ESR - results are colour coded for each technique). Note: the red TL and ESR error on the age estimates are presented at 1σ, while the U-series errors have been presented at 2 σ. **d**, The dating results modelled to constrain the breccia to 68 ± 5 (73-63) kyr.

METHODS

Teeth morphology and metrics
Measurements of the Lida Ajer teeth are taken from Hooijer[12] and, for the root robusticity and crown height of the M^2, measured from photographs scaled using the crown measurements (Extended Data Fig. 3). For the latter, root robusticity was measured using the method of Weidenreich[31] and crown height using the method of Moorrees[32]. Relative cusp areas of the molar were measured from a photograph of the occlusal surface using ImageJ software (Rasband, 1997–2008)[33]. The grade numbers referred to in the following are those defined in the Arizona State University Dental Anthropology System using their dental plaques[34].

Micro-CT relative enamel thickness (RET)
We applied microcomputed tomographic (micro-CT) imaging to assess the relative enamel thickness of the teeth (Extended Data Fig. 4). The teeth were scanned with a Skyscan 1172 micro-CT, and virtual sections planes were cut along the labio-lingual aspect of the incisor (11471) and across the mesial cusps of the molar (11472) following established protocols in[35-37]. Several variables were quantified on 2D section planes with Sigma Scan Pro software interfaced to a Wacom digitizing tablet following[38,39], enamel cap area (c), enamel-dentine junction length (e), and coronal dentine area enclosed by the enamel cap (b). Average enamel thickness (AET) was calculated as [c/e], yielding the average straight-line distance (mm units), or thickness, from the enamel-dentine junction to the outer enamel surface. AET was scaled for comparisons between taxa of different size by calculation of relative enamel thickness (RET): [100 * [c/e]/ sq. rt. b] (Supplementary Table 5).

Micro-CT Enamel-dentine junction (EDJ)
We followed a similar methodological approach described in Skinner *et al*.[40,41]. Briefly, each molar was microCT scanned at the Max Planck Institute for Evolutionary Anthropology in Leipzig, Germany using either an industrial or desktop microCT system with a resultant voxel resolution ranging from 14 – 70µm. The image stacks of each tooth were filtered (using a computer programmed macro that employs a three-dimensional median and mean-of-least-variance filter) to improve tissue grayscale homogeneity and then manually segmented into enamel and dentine components using Avizo (v6.1). The EDJ of each molar was extracted as a digital surface model (.ply format).

The EDJ surface models were imported into Avizo for the collection of three sets of 3D anatomical landmarks (Extended Data Fig. 4b). The first set (referred to as 'MAIN') included four landmarks: one on the tip of the dentine horn of each primary cusp. The second set includes landmarks (50–70) along the tops of the ridges that connect the four dentine horns. This set of points forms a continuous line, beginning at the tip of the protocone and moving in a buccal direction. The third set includes landmarks (~ 40) along the cervix of the molar, beginning at the midpoint of the buccal face and continuing in a lingual direction. As the ridge and cervix curves were later resampled (see below), it was not initially necessary that the same number of points be placed along the curve for each specimen. Thus, the spacing of points was dictated such that they did not touch adjacent neighbours, but was not so far apart as to misrepresent aspects of the curve (as represented in Extended Data Fig. 4b).

The process by which a corresponding set of landmarks and semilandmarks was generated for each specimen is outlined in SI – section 3. All data processing was done in Mathematica v6.0 (www. wolfram.com) using a software routine written by Philipp Gunz. We performed a principal component analysis (PCA) in shape and form space on the Procrustes coordinates of each specimen. We then used a cross-validated canonical variates analysis using inclusive sets of 10-24 principal components to determine the taxonomic affinity and molar position of the Lida Ajer molar.

Luminescence dating of quartz and feldspar grains

A bulk sediment sample (laboratory code LA-OSL1) for luminescence dating was collected using red-filtered torch light with additional samples for water content and environmental radioactivity determinations. Quartz grains of 90–125 µm in diameter were processed using standard purification procedures, including a final etch in 40% hydrofluoric acid for 45 mins to remove the external alpha-dosed rinds[42]. The LA1 sample yielded very small amounts of quartz – 60 mg, with ~20 mg used for Aliquot A and B to derive the D_e estimates (Supplementary Table 7), with only ~40 mg remaining for additional testing. In addition, 90–125 µm feldspar grains were etched in 10% hydrofluoric acid for 40 mins. Slightly more feldspar minerals were recovered than quartz so tests that are vital to the integrity of the final D_e could be conducted. All luminescence analysis was conducted at the 'Traps' luminescence dating facility at Macquarie University in Sydney, Australia.

In this region, the quartz is of volcanic origin so requires the use of a DAP red TL dating technique[43]. Quartz grains were mounted on stainless-steel discs using silicone oil spray, each large aliquot being composed of ~5000 grains (~10 mg). The isothermal red TL emissions[44-46] were measured using a red sensitive photomultiplier tube (Electron Tubes Ltd 9658B) and cooling tower (LCT50 liquid-cooled thermoelectric housing) with Kopp 2-63 and BG-39 filter combination[43], and laboratory irradiations were conducted using a calibrated $^{90}Sr/^{90}Y$ beta source. D_e were estimated from the 20–30 s interval of isothermal decay (which was bleachable by >380 nm illumination) using the final 160 s as background. Aliquots were heated to 260°C at a heating rate of 5 K s^{-1} and then held at 260°C for 1000 s to minimise the unwanted TL from incandescence. Palaeodoses were estimated from the 20–30 s interval of isothermal decay (which was bleachable by >380 nm illumination), using the final 160 s as background.

The ability to recover a known dose[47] was restricted by the small amounts of quartz present (60 mg), as seen in samples from Liang Bua in Flores[48], however, limited dose recovery experiments were conducted on 4 fresh aliquots. The natural signal was removed using an isothermal measurement (heated to 260°C and held for 1000 s) a surrogate dose of 50 Gy, a 1 hr bleach in a solar simulator and a second, larger dose (100 Gy) was applied and the surrogate D_e was estimated according to the DAP technique[43]. The surrogate doses for Aliquot A and B were recovered to within ~10% indicating that the standard 260°C preheat and isothermal measurement combination are appropriate for these samples. This result agrees with previous dose recovery procedures using DAP on a range of samples[43].

The feldspars in this volcanic region suffer from extreme anomalous fading[48], To overcome these problems we adopted a modified post-IR IRSL protocol (p-IR-IRSL) using a 300°C preheat and 270°C IRSL stimulation combination following a standard 50°C IR stimulation. pIR-IRSL measurements were conducted on feldspars using infrared (875 nm) light-emitted diodes (LEDs) at 80% power for 250 s and the emissions were detected using Schott BG-39 and Corning 7-59 filters to transmit wavelengths of 320–480 nm. Four procedural tests were applied to small aliquots of ~1000 grains using the following preheat and IR stimulation combinations; 250 and 225°C[49,50], 280 and 250°C[51], 300 and 270°C[51], and 320 and 290°C[52,53]; 1) a preheat plateau test using 3 discs; 2) fading tests including a prompt, 1 hour and 10 hour delay; 3) Bleaching tests using 1 fresh aliquot to determine the amount of residual IRSL after an extended bleach of 4 hours in a solar simulator and 4) dose recovery tests using 2 bleached aliquots (bleached using a solar simulator for 4 hours) and a surrogate dose of 200 Gy. From these tests it was determined that the 270°C stimulation and 300°C preheat combination provided the flattest preheat plateau, best recovery of the surrogate dose, least fading of all the pIR-IRSL signal (g value = 1.7 % per decade) and lowest residual value (8 Gy). 24 aliquots were used to conduct a modified SAR regenerative-dose procedure. The resulting D_e values

were corrected according to the results of residual dose estimation and anomalous fading tests (using a weighted mean fading rate of 1.7 ± 0.3 % per decade). Due to the sedimentary context of the cave we estimated the pIR-IRSL age of each sample using the minimum age model (MAM) divided by the environmental dose rate.

Measurements of ^{238}U, ^{235}U, ^{232}Th (and their decay products) and ^{40}K were estimated using Geiger-Muller multi-counter beta counting of dried and powdered sediment samples in the laboratory and a portable gamma spectrometer in the field. The corresponding (dry) beta and gamma dose rates were obtained using the conversion factors of Stokes *et al*.[54] and the beta-dose attenuation factors of [55], and an effective internal alpha dose rate of 0.03 Gy kyr^{-1} [56] and 0.72 Gy kyr^{-1} [57,58] for the 90-125 μm quartz and feldspar samples, respectively (due to the radioactive decay of ^{40}K and ^{87}Rb), which were made assuming K (13 ± 1 %[91]) and Rb (400 ± 100 μg g–1[58]) concentrations, and was included in the total dose rate. Cosmic-ray dose rates were estimated from published relationships[59], making allowance for the density and 8 m thickness of the limestone roof above the cave deposit, the geometry of the limestone shielding, the sediment overburden at the sample locality (~2.45-4.20 m), the altitude (~600 m above sea level) and geomagnetic latitude and longitude (0° and 100°) of the sampling site. The total dose rate was calculated using a long-term water content of 15 ± 5%, which is close to the measured (field) water content of 16%.

Uranium-series dating of speleothems

Calcite crystals free of any weathered surfaces were extracted from each of the above samples and cleaned ultrasonically to remove as much as possible sediment contamination before they were subjected to chemical treatment and isotopic measurements by mass spectrometry[60]. Uranium-series dating of the speleothem samples was conducted in the Radiogenic Isotope Facility of The University of Queensland using VG Sector 54 thermal ionisation mass spectrometer (TIMS) and a Nu Plasma multi-collector inductively coupled mass spectrometer (MC-ICP-MS). Analytical procedures follow[60] and [61,62] for TIMS and MC-ICP-MS, respectively. ^{230}Th/^{234}U ages were calculated using Isoplot EX 3.75[63] and half-lives of 75,690 years (^{230}Th) and 245,250 years (^{234}U)[64].

Laser ablation MC-ICPMS analysis of fossil teeth

We analyzed four primate teeth (two *Pongo* sp. and two Siamang gibbon) selected from our excavation at Lida Ajer and housed in the collection at the Indonesian National Centre for Archaeology in Jakarta (ARKENAS) (Extended Data Fig. 8a-d). In addition, we analysed a *Pongo* sp. tooth from Dubois's original excavation collection (9967/A), which is housed in Naturalis Museum in the Netherlands. The samples were analyzed for U-series isotopes at the Research School of Earth Sciences U-series laboratory at the Australian National University, Australia. The teeth were cut using a rotatory tool equipped with a thin (100 μm) diamond saw blade and samples were mounted into Al cups with the cross-section surfaces facing up to the top of the sample holder, corresponding to the focal point of the laser in the sampling cell (Extended Data Fig. 8e-h).

Uranium-series isotopic analyses of the teeth were carried out using a Finnigan MAT Neptune MC ICPMS equipped with multiple ion counters. Two ion counters were set to masses of 230.1 and 234.1. Faraday cups were set to collect the following masses: 232, 235, and 238. Laser sampling employed a Lambda Physik LPFPro ArF excimer laser source which lase at λ=193 nm. The laser source is coupled to the Neptune MC-ICPMS instrument through an ANU-designed Helex ablation cell. Details of the instrumentation analysis procedure have been modified from those reported in [65] and are reported in detail in [66].

The analyses were carried out with the laser spot size set to 265 μm using a 5 Hz pulse rate. The samples were initially cleaned for 5 s and ablation pits were measured for 50 s. Analyses were made

at regular spacing (typically 2 or 3 mm) along traverses that were computer programmed across regions of interest on cut tooth sections. The analyses made along each transect were bracketed between reference standard analyses to correct from instrument drift.

Semi-quantitative analysis of U and Th concentrations were derived alongside repeated measurements of two standards: SRM NIST-610 glass (U = 461.5 μg/g; Th = 457.2 μg/g), and rhinoceros tooth dentine from Hexian (sample 1118, see [67]). Age estimates were calculated using the Isoplot program[68].

Coupled US/ESR dating on fossil teeth

We applied direct ESR dating to two teeth (13/LA/5/08 and 12/LA/5/08) to enable coupled US/ESR analysis[69,70] conducted at the ESR laboratory at Southern Cross University, Lismore, Australia. From each sample, a fragment of enamel was extracted with the same diamond saw, and stripped from any attached dentine and calculus on the surface. The enamel and dentine were separated and the first 100μm of the enamel was removed on both sides (the Dentine-Enamel Junction (EDJ) and the occlusal surface). Both, LA-ICPMS (Agilent 7700 and ESI NW213) and LA-MC-ICPMS (Thermo Neptune plus and ESI NW193) analyses were performed directly on the enamel fragment and on the dentine in contact, to estimate the uranium content. U-series analyses were conducted using large rasters on both sides of the enamel fragment and all the way along the dentine from the EDJ to the root canal. The *in-situ* dosimetry used for the ESR dating was extracted from the OSL dosimetry conducted at the site (SI section 4**)**. Sediment content for U, th and k was estimated from activity values using ^{238}U: 1 Bq/kg = 81 ppb; ^{232}Th=1 Bq/kg = 246 ppb; ^{40}K= 1 Bq/kg = 0.00323%.

ESR dating was performed on a Freiberg MS5000 X-band (2mw microwave power, 0.1mT modulation amplitude) with goniometer 1300 with a 10 degree step, and irradiated with an x-ray source ionization chamber from Freiberg (40kv at 0.5mA). The source is a stable x-ray gun Varian VF50 integrated in a homogenised irradiation chamber (designed by Freiberg instrument). The emission consistency was tested on alanine dosimeter and the dose calibrated against gamma irradiation directly on tooth enamel (fossil and modern, unpublished data). The dose response curve (DRC), which represents the radiation sensitivity and susceptibility of the sample, is extrapolated to cross the x-axes, indicating the D_e. The dose is described, as equivalent since it is determined using either laboratory gamma or x-ray irradiation, while the actual dose received in nature is the sum of all radiations from multi-energetic emissions α, β, γ and cosmic rays. Dose response curves (DRC) were calculated using MCDoseE 2.0 program a Markov Chain Monte-Carlo calculation-fitting algorithm (for more details see [71]). For the estimation of the equivalent dose (D_e), each fragment was irradiated 7 times, following exponentially increasing irradiation times (90, 380, 900, 1800, 3600, 7200 and 14400 s). During each irradiation step, the output of the X-ray gun was recorded, which allows the accurate calculation of the dose rate received by the sample (for 12/LA/508 and 13/LA/508 with average dose rates of 0.152 Gy/s and 0.254 Gy/s respectively). Isotropic and baseline corrections were applied uniformly across the measured spectra. The amount of NOCORs in the natural signal was estimated for potential correction (for more details see [71]). D_e values were obtained by fitting a single saturating exponential (SSE) at the appropriate maximum irradiation dose (D_{max}) following the recommendations for accurate DRC estimation[72] (using 12/LA/508 D_{max}= 2172 Gy and 13/LA/508 D_{max}= 3621 Gy). US/ESR age results were modelled using the Monte Carlo approach[73].

Bayesian modelling

To evaluate the uncertainties of the integrated dating approach (Extended Data Fig. 10b), Bayesian modelling was performed on all independent age estimates using the OxCal (version 4.2) software[74] available at https://c14.arch.ox.ac.uk /embed.php?File=oxcal.html. The analysis incorporated the

probability distributions of individual dates, and constraints imposed by stratigraphic relationships and the reported minimum/maximum nature of some of the individual age estimates. Each individual age was included as a Gaussian distribution (with mean and standard deviation defined by the age estimate and their associated uncertainties). The U-series profiling ages on the fossil Pongo and Siamang gibbon teeth yielded a range of dates (80-75 kyr) and these were incorporated as a uniform distribution over this interval. The age of the breccia deposit was conservatively estimated as the boundary age between the overlying calcite deposits and the age estimates from within the breccia deposit, incorporating all of the constraints described above (Extended Data Fig. 10b).

Data availability

The data that support the findings of this study are available from the corresponding author upon reasonable request (kira.westaway@mq.edu.au).

References

31. Weidenreich, F. The dentition of *Sinanthropus pekinensis*: A comparative odontography of the hominids (China. Geological survey Palaeontologia sinica, new ser. D) (1937).
32. Moorrees, C.F.A., 1957. *The Aleut Dentition*. (Harvard University Press, Cambridge, 1957).
33. Rasband, W. S. ImageJ. U. S. National Institutes of Health, Bethesda, Maryland, USA, http://rsb.info.nih.gov/ij/ (1997-2008).
34. Turner, C.G., Nichol, C.R. & Scott, G.R. Scoring procedures for key morphological traits of the permanent dentition: the Arizona State University dental anthropology system. In *Advances in Dental Anthropology* (ed. Kelly & Larsen) 13-31 (New York: Wiley-Liss, 1991).
35. Smith, T.M., Olejniczak, A.J., Reid, D.J., Ferrell, R.J., & Hublin, J.J. Modern human molar enamel thickness and enamel-dentine junction shape. *Arch. Oral Biol.* **51**, 947-995 (2006).
36. Smith, T.M., Bacon, A-M., Demeter, F., Kullmer, O., Nguyen, K.T., Vos, J. de, Wei, W., Zermeno, J.P. & Zhao, L. Dental tissue proportions in fossil orangutans from mainland Asia and Indonesia. *Human Origins Research* 1:-1 (doi: 10.4081/hor.2011.e1) (2011).
37. Smith, T.M., Kupczik, K., Machanda, Z., Skinner, M.M. & Zermeno JP. Enamel thickness in Bornean and Sumatran orangutan dentitions. *Am. J. Phys. Anthropol.* **147**, 417-426 (2012).
38. Martin, L.B. *Relationships of the later Miocene Hominoidea* (Ph.D. Dissertation, University College London, 1983).
39. Martin, L.B. Significance of enamel thickness in hominoid evolution. *Nature* **314,** 260-263 (1985).
40. Skinner, MM, Gunz, P, Wood, BA, & Hublin, J-J. Enamel-dentine junction (EDJ) morphology distinguishes the lower molars of *Australopithecus africanus* and *Paranthropus robustus*. *J. Hum. Evol.* **55**, 979-988 (2008).
41. Skinner, MM, Gunz, P, Wood, BA, & Hublin, J-J. Discrimination of extant Pan species and subspecies using the enamel-dentine junction morphology of lower molars. *Am. J. Phys. Anthropol.* **140**, 234-243 (2009).
42. Huntley, D.J., Godfrey-smith, D.I. & Thewalt, M.L.W. Optical dating of sediments. *Nature* **313**, 105-107 (1985).
43. Westaway, K. E., & Roberts, R. G. A dual-aliquot regenerative-dose protocol (DAP) for thermoluminescence (TL) dating of quartz sediments using the light-sensitive and isothermally-stimulated red emissions. *Quaternary Sci. Rev.* **25**, 2513-2528 (2006).
44. Spooner, N.A. & Franklin, A.D. Effect of the heating rate on the red TL of quartz. *Radiat. Meas.* **35**, 59-66 (2002).
45. Murray, A.S. & Mejdahl, V. Comparison of regenerative-dose single-aliquot and multiple-aliquot (SARA) protocols using heated quartz from archaeological sites. *Quaternary Sci. Rev.* **18**, 223-229 (1999).
46. Huot, S., Buylaert, J.P. & Murray, A.S. Isothermal thermoluminescence signals from quartz. *Radiat. Meas.* **41**, 796-802 (2006).
47. Murray, A.S. & Wintle, A.G. Luminescence dating of quartz using an improved single-aliquot regenerative-dose protocol. *Radiat. Meas.* **32**, 57-73 (2000).
48. Morwood, M. J., Soejono, R. P., Roberts, R. G., Sutikna, T., Turney, C. S. M., Westaway, K. E., Rink, W. J., Zhao, J.-x., van den Bergh, G. D., Awe Due, R., Hobbs, D. R., Moore, M. W., Bird, M. I., & Fifield, L. K.

Archaeology and age of a new hominin species from Flores in eastern Indonesia. *Nature* **431**, 1087–1091 (2004).
49. Thompsen, K.J., Murray, A.S., Jain, M., & Botter-Jensen, L. Laboratory fading rates of various luminescence signals from feldspar-rich sediment extracts. *Radiat. Meas*. **43**, 1474-1486 (2008).
50. Murray, A.S., Buylaert, J.P., Thomsen, K.J., & Jain, M. The effect of preheating on the IRSL signal from feldspar. *Radiat. Meas.* **44**, 554-559 (2009).
51. Thiel, C., Buylaert, J.-P., Murray, A., Terhorst, B., Hofer, I., Tsukamoto, S., & Frechen, M. Luminescence dating of the Stratzing loess profile (Austria); Testing the potential of an elevated temperature post-IR IRSL protocol. *Quatern. Int.* **234**, 23-31 (2011).
52. Thomsen, K.J., Murray, A.S., & Jain, M. Stability of IRSL signals from sedimentary K-feldspar samples. *Geochronometria* **38**, 1-13 (2011).
53. Buylaert, J.P., Murray, A.S., Thomsen, K.J., & Jain, M. Testing the potential of an elevated temperature IRSL signal from K-feldspar. *Radiat. Meas*. **44**, 560-565 (2009).
54. Stokes, S., Ingram, S., Aitken, M.J., Sirocko, F., Anderson, R. & Leuschner, D. Alternative chronologies for Late Quaternary (Last Interglacial-Holocene) deep sea sediments via optical dating of silt-sized quartz. *Quaternary Sci. Rev.* **22**, 925–941 (2003).
55. Mejdahl, V. Thermoluminescence dating: beta-dose attenuation in quartz grains. *Archaeometry* **21**, 61–72 (1979).
56. Feathers, J.K. & Migliorini, E. Luminescence dating at Katanda – a reassessment. *Quaternary Sci. Rev.* **20**, 961-966 (2001).
57. Huntley, D.J., & Baril, M.R. The K content of the K-feldspars being measured in optical dating or in thermoluminescence dating. *Anc. TL* **15**, 11-13 (1997).
58. Huntley, D.J., & Hancock, R.G.V. The Rb contents of the K-feldspars being measured in optical dating. *Anc. TL* **19**, 43-46 (2001).
59. Prescott, J.R. & Hutton, J.T. 1994. Cosmic-ray contributions to dose-rates for luminescence and ESR dating - large depths and long-term time variations. *Radiat. Meas.* **23**, 497-500 (1994).
60. Zhao, J.-x., Hu, K., Collerson, K. D. & Xu, H.-k. 2001. Thermal ionization mass spectrometry U-series dating of a hominid site near Nanjing, China. *Geology* **29**, 27-30 (2001).
61. Zhou, H.Y., Zhao, J.X., Wang, Q., Feng, Y.X. & Tang, J. Speleothem-derived Asian summer monsoon variations in Central China during 54-46 ka. *J. Quaternary Sci.* **26**, 781–790 (2011).
62. Clark, T.R., Zhao, J.X., Roff, G., Feng, Y.X., Done, T.J., Nothdurft, L.D. & Pandolfi, J.M. Discerning the timing and cause of historical mortality events in modern Porites from the Great Barrier Reef. *Geochimica Et Cosmochimica Acta* **138**, 57–80 (2014).
63. Ludwig, K.R. User's Manual for Isoplot 3.75. *A Geochronological Toolkit for Microsoft Excel*. (Berkeley Geochronology Center Special Publication No. 5, 2012).
64. Cheng, H., Edwards, R. L., Hoff, J., Gallup, C. D., Richards, D. A. & Asmerom, Y. The half-lives of uranium-^{234} and thorium-^{230}. *Chemical Geology* **169**, 17-33 (2000).
65. Eggins, S.M., Grün, R., McCulloch, M.T., Pike, A.W.G., Chappell, J., Kinsley, L., Shelley, M., Murray-Wallace, C.V., Spötl, C. & Taylor, L. In situ U-series dating by laser-ablation multi-collector ICPMS: new prospects for Quaternary geochronology. *Quaternary Sci. Rev.* **24**, 2523-2538 (2005).
66. Grün, R., Eggins, S., Kinsley, L., Moseley, H., & Sambridge, M. Laser ablation U-series analysis of fossil bones and teeth. *Palaeogeogr. Palaeocl. Palaeoecol*. DOI: 10.1016/j.palaeo.2014.07.023 (in press).
67. Grün, R., Huang, P.H., Huang, W., McDermott, F., Stringer, C.B., Thorne, A., & Yan, G. ESR and U-series analyses of teeth from the palaeoanthropological site of Hexian, Anhui Province, China. *J. Hum. Evol.* **34**, 555-564 (1998).
68. Ludwig, K.R. User's Manual for Isoplot 3.00, Manual. Berkeley Geochronology Center: Berkeley, CA (2003).
69. Joannes-Boyau, R. Detailed protocol for accurate non-destructive direct dating of human remains. *Geochronometria* **40**, 322-333 (2013).
70. Joannes-Boyau, R. & Bodin, T. *MCDEC program: a Monte-Carlo dose equivalent calculation program*. (Unpublished report, 2013).
71. Duval, M., Grün, R. Are published ESR dose assessments on fossil tooth enamel reliable? *Quat. Geochronol.* **31**, 19-27 (2016).
72. Shao, Q., Bahain, J.J., Falgueres, C., Dolo, J.M. & Garcia, T. A new U-uptake model for combined ESR/U-series dating of tooth enamel. *Quat. Geochronol.* **10**, 406-411 (2014).

73. Guérin, G., Mercier, N., Adamiec, G. Dose rate conversion factors: update. *Ancient TL* **29**, 5-8 (2011).
74. Bronk, R.C. Radiocarbon calibration and analysis of stratigraphy: The OxCal program. *Radiocarbon* **37**, 425-430 (1995).
75. Shen, G., Wang, W., Wang, Q., Zhao, J., Collerson, K.D., Zhou, C., Tobias, P.V., 2002. U-Series dating of Liujiang hominid site in Guangxi, Southern China. *J. Hum. Evol.* **43**, 817-829.
76. Kahlke, H.D., 1961. On the complex of the Stegodon-Ailuropoda-Fauna of South China and the chronological position of *Gigantopithecus blacki* Von Koenigswald. *Vertebrata Palasiatica* **2**, 83-108.
77. deVos, J., Long, Vu. In: Semah, F., et al., (Eds.) *Origins of settlements and chronology of the Palaeolithic cultures in Southeast Asia*, (Semenajung, Paris, 2001).
78. Ciochon, R. L. & Larick, R. Dated co-occurrence of *Homo erectus* and *Gigantopithecus* from Tham Khuyen Cave, Vietnam. *P. Natl. Acad. Sci. U.S.A.* **93**, 3016 (1996).
79. Cuong, N.L. Fossile Menschenfunde aus Nordvietnam. In: Herrmann, J., and Ullrich, H., (Eds.) *Menschwerdung – Biotischer und Gesellschafrlicher Entwicklungs* – (Prozess. Akademie Verlag, Berlin, 1985).
80. Bacon, A.-M., Demeter, F., Schuster, M., Long, V.T., Thuy, N., K., P.-O., A., Sen, S., Nga, H.H., Huong, N.M. The Pleistocene Ma U'Oi cave, northern Vietnam: palaeontology, sedimentology and palaeoenvironments. *Geobios* **37**, 305-314 (2004).
81. de Vos, J., 2007. Mid-Pleistocene of Southern Asia, In: Elias, S.A. (Ed.), *The Encyclopedia of Quaternary Science* (Elsevier, Oxford, 2007).
82. Tougard, C., Jaeger, J.J., Chaimanee, Y., Suteethorn, V., Triamwichanon, S. Discovery of a *Homo* sp. tooth associated with a mammalian cave fauna of Late Middle Pleistocene age, Northern Thailand. *J. Hum. Evol.* **35**, 47-54 (1998).
83. Barker, G., Barton, H., Bird, M., Daly, P., Datan, I., Dykes, A., Farr, L., Gilbertson, D., Harrisson, B., Hunt, C., Higham, T., Kealhofer, L., Krigbaum, J., Lewis, H., McLaren, S., Paz, V., Pike, A., Piper, P., Pyatt, B., Rabett, R., Reynolds, T., Rose, J., Rushworth, G., Stephens, M., Stringer, C., Thompson, J., & Turney, C. The 'human revolution' in lowland tropical Southeast Asia: the antiquity and behavior of anatomically modern humans at Niah Cave (Sarawak, Borneo). *J. Hum. Evol. Evolution* **52**, 243-261 (2007).
84. de Vos, J., 1983. The Pongo faunas from Java and Sumatra and their significance for biostratigraphical and paleo-ecological interpretations. *Proceedings of the Koninklijke Nederlandse Akademie van Wetenschappen Series B* **86**, 417-425.
85. Dennell, R. & Roebroeks, W. An Asian perspective on early human dispersal from Africa. *Nature* **438**, 1099-1104 (2005).
86. Glover, I. Leang Burung 2: An upper Palaeolithic rock shelter in South Sulawesi, Indonesia. Modern *Quaternary Research in Southeast Asia* **6**, 1-38 (1981).
87. Anderson, D. D. A Pleistocene-early Holocene rock shelter in peninsular Thailand. *National Geographic Research* **3**, 184-198 (1987).
88. Duringer, P., Bacon, A.-M., Sayavongkhamdyc, T., & Nguyen Thi Kim Thuy. Karst development, breccias history, and mammalian assemblages in Southeast Asia: A brief review. *Comptes Rendus Palevol 11*, 133-137 (2012).
89. Dubois, E. Voorloopig bericht omtrent het onderzoek naar de Pleistocene en tertiaire Vertebraten-Fauna van Sumatra en Java, gedurende het jaar 1890. Natuurk. Tijdschr. Ned. Ind. 51, 93-100 (1891).
90. Dubois, E. Das geologische Alter der Kendeng-oder Trinil fauna. *Tijdschrift Koninklijke Nederlandsch Aardrijkskundig Genootschap* series 2 25, 1235–1270 (1908).
91. Wu, X. & Zhang, Z. *Homo sapiens* remains from Late Palaeolithic and Neolithic China. (In Wu, R. & Olsen, J. W. *Palaeoanthropology and Palaeolithic Archaeology in the People's Republic of China*) 107-133 (Academic Press, London, 1985).
92. Black, G.V. *Descriptive anatomy of the human teeth*. (Fifth Edition. SS White Dental Manufacturing Company. Philadelphia, 1902).
93. Jianing, H., 2000. Preliminary study on the teeth of Jinniushan archaic *Homo sapiens*. *Acta Anthropologica Sinica*, **3**, 006 (2000).
94. Etler, D.A., Crummett, T.L. & Wolpoff, M.H. Longgupo: Early *Homo* colonizer or late Pliocene *Lufengpithecus* survivor in south China? *Human Evolution* **16**, 1-12 (2001).
95. Liu, W. The dental morphology and continuity of prehistoric and historic humans of China. *Interdisciplinary Perspectives on the Origins of the Japanese* **11**, 43-64 (1999).

96. Wu, X. & Poirier, F.E. *Human evolution in China: a metric description of the fossils and a review of the sites*. Oxford University Press, USA (1995).
97. van den Bergh, G.D., Kaifu, Y., Kurniawan, I., Kono, R.T., Brumm, A., Setiyabudi, E., Aziz, F. & Morwood, M.J. *Homo floresiensis*-like fossils from the early Middle Pleistocene of Flores. *Nature* **534**, 245-248 (2016).
98. Kaifu, Y., Kono, R.T., Sutikna, T., Saptomo, E.W., Awe, R.D. & Baba, H. Descriptions of the dental remains of *Homo floresiensis*. *Anthropological Science* **123**, 129-145 (2015).
99. Williams, J.L. A new classification of human tooth forms; with special reference to a new system of artificial teeth. *Dental Digest* **XX**, 63-67 (1914).
100. Zaim, Y., Ciochon, R.L., Polanski, J.M., Grine, F.E., Bettis, E.A., Rizal, Y., Franciscus, R.G., Larick, R.R., Heizler, M., Eaves, K.L. & Marsh, H.E. New 1.5 million-year-old *Homo erectus* maxilla from Sangiran (Central Java, Indonesia). *J. Hum. Evol. Evolution* **61**, 363-376 (2011).
101. Alqahtani, S.J., Hector, M.P. & Liversidge, H.M. Brief communication: the London atlas of human tooth development and eruption. *Am. J. Phys. Anthropol.* **142**, 481-490 (2010).
102. Hillson, S., 1996. *Dental anthropology* (Cambridge University Press 1996).
103. Xing, S., Martinón-Torres, M., Bermúdez de Castro, J.M., Wu, X. & Liu, W. Hominin teeth from the early Late Pleistocene site of Xujiayao, Northern China. *Am. J. Phys. Anthropol.* **156**, 224-240 (2015).
104. Brace, C.L. & Vitzthum, V. Human tooth size at Mesolithic, Neolithic and modern levels at Niah Cave, Sarawak: comparisons with other Asian populations. (The) *Museum Journal Kuching (Sarawak)* **33**, 75-82 (1984).
105. Jacob, T. Studies on human variation in Indonesia. *Journal of the National Medical Association* **66**, 389 (1974).
106. Sarasin, P. Neue lithochrone Funde im Innern von Sumatra. *Verh. naturf. Ges. Basel* **25**, 97-111 (1914).
107. Xing, S., Sun, C., Martinón-Torres, M., de Castro, J.M.B., Han, F., Zhang, Y. & Liu, W. Hominin teeth from the Middle Pleistocene site of Yiyuan, Eastern China. *J. Hum. Evol.* **95**, 33-54 (2016).
108. Xing, S., Martinón-Torres, M., de Castro, J.M.B., Zhang, Y., Fan, X., Zheng, L., Huang, W. & Liu, W. Middle Pleistocene hominin teeth from Longtan Cave, Hexian, China. *PloS one* **9**, e114265 (2014).
109. Liu, W., Schepartz, L.A., Xing, S., Miller-Antonio, S., Wu, X., Trinkaus, E. & Martinón-Torres, M. Late middle Pleistocene hominin teeth from Panxian Dadong, South China. *J. Hum. Evol.* **64**, 337-355 (2013).
110. Bailey, S.E. The evolution of non-metric dental variation in Europe. *Mitteilungen der Gesellschaft für Urgeschichte* **15**, 9-30 (2006).
111. Liu, W., Wu, X., Pei, S., Wu, X. & Norton, C.J. Huanglong Cave: a late Pleistocene human fossil site in Hubei Province, China. *Quatern. Int.* **211**, 29-41 (2010).
112. Bermúdez de Castro, J. M., Rosas, A. & Nicolás, M.E. Dental remains from Atapuerca-TD6 (Gran Dolina site, Burgos, Spain). *J. Hum. Evol.* **37**, 523–566 (1999).
113. Irish, J.D. & Guatelli-Steinberg, D. Ancient teeth and modern human origins: an expanded comparison of African Plio-Pleistocene and recent world dental samples. *J. Hum. Evol.* **45**, 113-144 (2003).
114. Irish, J.D. Ancestral dental traits in recent Sub-Saharan Africans and the origins of modern humans. *J. Hum. Evol.* **34**, 81-98 (1998).
115. Scott, G.R. & Turner II, C.G. *The Anthropology of Modern Human Teeth: Dental Morphology and its Variation in Recent Human Populations*. Cambridge University Press. Cambridge, England (1997).
116. Kaifu, Y., Kono, R.T., Sutikna, T., Saptomo, E.W. & Awe, R.D. Unique dental morphology of *Homo floresiensis* and its evolutionary implications. *PloS one* **10**, p.e0141614 (2015).
117. Shen, G., Wu, X., Wang, Q., Tu, H., Feng, Y.X. & Zhao, J.X. Mass spectrometric U-series dating of Huanglong Cave in Hubei Province, central China: evidence for early presence of modern humans in eastern Asia. *J. Hum. Evol.* **65**, 162-167 (2013).
118. Bailey, S.E. & Liu, W. A comparative dental metrical and morphological analysis of a Middle Pleistocene hominin maxilla from Chaoxian (Chaohu), China. *Quatern. Int.* **211**, 14-23 (2010).
119. Wu, R.K. & Dong, X.R. The fossil human-teeth from Yunxian, Hubei. *Vertebrata PalAsiatica*, **18**, 142-149 (1980).
120. Grine, F.E. & Franzen, J.L. Fossil hominid teeth from the Sangiran dome (Java, Indonesia). *Courier Forsch Senckenberg* **171**, 75-103 (1994).
121. Wood, B.A. *Koobi Fora research project IV: hominid cranial remains from Koobi Fora*. (Clarendon, Oxford, 1990).

122. Indriati, E. and Antón, S.C. Earliest Indonesian facial and dental remains from Sangiran, Java: a description of Sangiran 27. *Anthropological Science* **116**, 219-229 (2008).
123. Demeter, F., Shackelford, L., Westaway, K., Duringer, P., Bacon, A.M., Ponche, J.L., Wu, X., Sayavongkhamdy, T., Zhao, J.X., Barnes, L. & Boyon, M. Early modern humans and morphological variation in Southeast Asia: fossil evidence from Tam Pa Ling, Laos. *PloS one* **10**, e0121193 (2015).
124. Demeter, F., Shackelford, L., Bacon, A.M, Duringer, P., Westaway, K.E., Sayavongkhamdy, T., Braga, J., Sichanthongtip, P., Khamdalavong, P., Ponche, J-L, Lundstrom, C, Patole-Edoumba, E, 52, & Karpoff, A-M, 2012. Anatomically modern human in Southeast Asia (Laos) by 46 ka. *P. Natl. Acad. Sci. U.S.A* **109**, 14375-1438 (2012).
125. Bae, C.J., Wang, W., Zhao, J., Huang, S., Tian, F. & Shen, G. Modern human teeth from Late Pleistocene Luna Cave (Guangxi, China*). Quatern. Int.* **354**, 169-183 (2014).
126. Matsumura, H., Yoneda, M., Dodo, Y., Oxenham, M.F., Cuong, N.L., Thuy, N.K., Dung, L.M., Long, V.T., Yamagata, M., Sawada, J. & Shinoda, K. Terminal Pleistocene human skeleton from Hang Cho Cave, northern Vietnam: implications for the biological affinities of Hoabinhian people. *Anthropological Science* **116**, 201-217 (2008).
127. Matsumura, H., Cuong, N.L., Thuy, N.K. & Anezaki, T. Dental morphology of the early Hoabinian, the Neolithic Da But and the Metal Age Dong Son civilized peoples in Vietnam. *Zeitschrift für Morphologie und Anthropologie*, 59-73 (2001).
128. Matsumura, H. & Pookajorn, S. A morphometric analysis of the Late Pleistocene human skeleton from the Moh Khiew Cave in Thailand. *Journal of Comparative Human Biology* **56**, 93-118 (2005).
129. Bae, C.J., 2010. The late Middle Pleistocene hominin fossil record of eastern Asia: synthesis and review. *Am. J. Phys. Anthropol.* **143**, 75-93 (2010).
130. Matsumura, H. & Hudson, M.J. Dental perspectives on the population history of Southeast Asia. *Am. J. Phy. Anthropol.* **127**, 182-209 (2005).
131. Matsumura, H. & Zuraina, M. Metrical analysis of the dentition of Perak man from Gua Gunung Runtuh in Malaysia. *Bulletin of the National Science Museum*, Tokyo, Series D, **21**, 1-10 (1995).
132. Jacob, T. *Some problems pertaining to the racial history of the Indonesian region: A study of human skeletal and dental remains from several prehistoric sites in Indonesia and Malaysia.* (University of Utrecht, 1967).
133. Storm, P. *The evolutionary significance of the Wajak skulls*. (Nationaal Natuurhistorisch Museum, 1995).
134. Groesbeek, B.J. The serial position of the Trinil upper molars. *Anthropological Science* **104**, 107–130 (1996).
135. Smith, T.M., Olejniczak, A.J., Kupczik, K., Lazzari, V., Vos, J., Kullmer, O., Schrenk, F., Hublin, J.-J., Jacob, T. & Tafforeau, P. Taxonomic assessment of the Trinil molars using non-destructive 3D structural and developmental analysis. *PaleoAnthropology* 117–129 (2009).
136. Ciochon, R.L. Divorcing hominins from the Stegodon-Ailuropoda fauna: new views on the antiquity of hominins in Asia. In: Out of Africa I: *The First Hominin Colonization of Eurasia* (J.G. Fleagle, J.J. Shea, F.E. Grine, A.L. Baden, R.E. Leakey Eds) 111-126 (Vertebrate Paleobiology and Paleoanthropology, Dordrecht, Springer, 2010).
137. Gunz, P, Mitteroecker P, & Bookstein F.L. Semilandmarks in three dimensions. In: *Modern Morphometrics in Physical Anthropology* (ed. Slice DE) 73–98 (New York: Kluwer Academic⁄Plenum Publishers 2005).
138. Westaway, K.E. The red, white and blue of quartz luminescence: A comparison of D_e values derived for sediments from Australia and Indonesia using thermoluminescence and optically stimulated luminescence emissions. *Radiat. Meas.* **44**, 462-466 (2009).
139. Ibrahim, Y., Tshen, L.T, Westaway, K.E., Earl of Cranbrook, Peng, L.C., Muhammad, R.F. & Humphrey. L. First records of fossils of Orangutan Pongo Sp. of Quaternary age from Peninsular Malaysia. *J. Hum. Evol.* **65**, 770-797 (2013).
140. Roberts, R.G., Westaway, K.E., Zhao, J.-x., Turney, C.S.M., Bird, M.I., Rink, W.J., & Fifield, L.K. Geochronology of cave deposits at Liang Bua and of adjacent river terraces in the Wae Racang valley, western Flores, Indonesia: a synthesis of age estimates for the type locality of *Homo floresiensis*. *J. Hum. Evol.* **57**, 484-502 (2009).
141. Wintle, A.G. Anomalous fading of thermoluminescence in mineral samples. *Nature* **245**, 143-144 (1974).
142. Olley, J.M., Murray, A. & Roberts, R.G. The effects of disequilibria in the uranium and thorium decay chains on burial dose rates in fluvial sediments. *Quaternary Sci. Rev.* **15**, 751-760 (1996).

143. Olley, J.M., Roberts, R.G. & Murray, A.S. Disequilibria in the uranium decay series in sedimentary deposits at Allen's Cave, Nullarbor Plain, Australia: Implications for dose rate determinations. *Radiat. Meas.* **27**, 433-443 (1997).
144. St Pierre, E., Zhao, J.-X. & Reed, E. Expanding the utility of uranium-series dating of speleothems for archaeological and palaeontological applications. *J. Archaeol. Sci.* **36**, 1416-1423 (2009).
145. St Pierre, E., Zhao, J.-X., Feng, Y.-X. & Reed, E., 2012. U-series dating of soda straw stalactites from excavated deposits: method development and application to Blanche Cave, Naracoorte, South Australia. *J. Archaeol Sci.* **39**, 922-930 (2012).
146. Millard, A.R. *Diagenesis of Archaeological Bone: The Case of Uranium Uptake*. (D.Phil. thesis, University of Oxford, 1993).
147. Millard, A.R. & Hedges, R.E.M. A diffusion-adsorption model of uranium uptake by archaeological bone. *Geochim. Cosmochim. Acta* **60**, 2139-2152 (1996).
148. Pike, A.W.G. *Uranium Series Dating of Archaeological Bone by Thermal Ionization Mass Spectrometry* (D.Phil. thesis, University of Oxford, 2000).
149. Pike, A.W.G., Hedges, R.E.M. & Van Calsteren, P. U-series dating of bone using the diffusion-adsorption model. *Geochim. Cosmochim. Acta* **66**, 4273-4286 (2002).
150. Sambridge, M., Grün, R. & Eggins, S. U-series dating of bone in an open system: the diffusion-adsorption-decay model. *Quat. Geochronol.* **9**, 42-53 (2012).
151. Grün, R. & McDermott, F. 1994. Open system modelling for U-series and ESR dating of teeth. *Quat. Geochronol.* **13**, 121–125 (1994).

Extended Data Figures legends

Extended Data Figure 1: Southeast Asian fossil sites and Dubois' Lida Ajer. **a**, Corridor dispersal of fauna into Southeast Asia during periods of connection (redrawn with permission from[7]). **b**, The main fossil faunal sites in Southeast Asia; in southern China; 1. Luijiang, 2. Liucheng, 3. Hoshantung, 4. Hei-Tu'ung, 5. Changyang, 6. Hsing-an. In Vietnam; 7. Lang Trang, 8. Tham Khuyen, 9. Thung Lang, 10. Hang Hum, 11. Ma U 'Oi, 12. Tham Om, 13. Keo Leng. In Laos; 14. Tham Hang, 15. Tham P'a Loi. In Thailand; 16.Thum Wiman Nakin, 17.Thum Phra Khai Phet. In Cambodia; 18. Phnom Loang. In Borneo; 19. Niah Cave. In Indonesia; 20. Lida Ajer, 21. Sibrambang, 22. Punung (redrawn with permission from[7]). **c**, Dubois's field sketches of Lida Ajer cave location copied directly from his field notebook - now housed in Leiden (with kind permission from Naturalis, Netherlands). His rough sketch of the cave location close to Payakumbuh village have had annotations added to make the features clearer. **e**, Our map of the cave location for comparison, note the similar relationship between Mount Sago, River Agam and Lida Ajer. **f**, Dubois's plan of the cave, annotations have been added to identify the chambers discussed in the text. **g**, Our plan of the cave for comparison, with the only differences being the absence of the sinkhole passage on our plan (unmapped).

Extended Data Figure 2: Fauna and speleothems from minor excavations at Lida Ajer in 2007. a) Cervid sp. b) Cervid sp. c) *Pongo* sp. upper premolar d) *Rusa* sp., e) *Pongo* sp. molar, f) *Pongo* sp. molar mesial view from d, g) Siamang gibbon molar; h) *Pongo* sp. molar mesial view from e, i) *Hystrix* sp., j) soda straw stalactite samples LA08-29 (own scale on photograph). k, Photograph of Areas 3 and 4 in the cave where the majority of fossil fauna were discovered.

Extended Data Figure 3: The fossil human teeth from Lida Ajer Cave and associated metrics. **a**, The incisor and **b**, molar mesiodistal versus buccolingual metrics plotted against data from 37 and 353 fossil *Pongo* teeth[16], respectively. **c**, incisor and **d**, molar data are plotted against the full range of *Homo* teeth from African early *Homo* to recent modern (data from Xing *et al*.[25]). In all four plots the Lida Ajer teeth are denoted by a red star, while the key for symbols (c-d) representing the different human teeth are in the inset box. **e**, The incisor and **f**, The molar from Lida Ajer.

Extended Data Figure 4: Micro-CT of the Lida Ajer teeth. **a**, Virtual sections of the Lida Ajer teeth. The labio-lingual section of the incisor is on the left, the bucco-lingual section through the mesial molar cusps in the on the right. The scale bar is equal to 5 mm. **b**, EDJ anatomical landmarks. Landmark protocol for geometric morphometric analysis of EDJ shape. Numbers in brackets represent the number of equidistantly spaced landmarks between main landmarks (red spheres) and around the cervix.

Extended Data Figure 5: Internal and external structure of the Lida Ajer teeth. CT-based volume renderings of the external surface (left) and surface models of the enamel-dentine junction (right) of the Lida Ajer molar in six anatomical views. At bottom, initial landmark placement (yellow spheres) capturing the main dentine horns, EDJ ridge and cervix (left) and noting the presence of an accessory dentine horn mesial to the metacone (left).

Extended Data Figure 6: Principal component analysis of EDJ shape of the comparative sample and the Lida Ajer molar.

Extended Data Figure 7: Example of the red TL and pIR-IRSL data for sample LA-1; (a, b) a comparison of the red TL signal characteristics using glow curves derived from a Liang Bua sample WR1 (a) and from the Lida Ajer sample (b). The glow curves demonstrate that after 500 Gy dosing the low temperature peaks disappear with the introduction of the 260°C preheat, and the presence of a light sensitive shoulder (260-305°C) that is removed by 1 hour of bleaching. The Lida Ajer sample shows similarities with the Liang Bua sample but has a more defined bleachable shoulder and a more intense signal; (c) Isothermal decay of the red TL signal from sample LA-1; (d) dose response curve for the unbleachable signal derived from aliquot 1 providing a D_e of 132 ± 13 Gy (see Westaway and Roberts, 2006 for further methodological details). **e**, pIR-IRSL intensity and shine down from red diodes stimulation for 250 s at 270°C, displaying the natural and a regenerative dose for comparison, **f**, pIR-IRSL sensitivity corrected dose response providing a D_e of 103 ± 9 Gy. **g**, The D_e values of the 22 aliquots of feldspars plotted on a radial plot. Each aliquot was corrected for minor fading and residual dose and was plotted producing an overdispersion of 17.6%. Prior to running the minimum age model (MAM) a value of 10% was added to the errors as an estimation of inherent overdispersion within the grains. This was determined by estimating the distribution of D_e values of 12 aliquots after a 4 hr bleach in a solar simulator. The MAM produced a D_e of 105 ± 3 Gy as depicted by a solid black line, which lies within ± 10% of the Central age (shaded box) due to the low overdispersion. This produces an age estimate of 62 ± 5 kyr. **h**, Fading tests for the Lida Ajer feldspars comparing the IR_{50} measurement with a g value of 17.67 with the $pIR\text{-}IRSL_{270}$ measurement, which has reduced the g value to 1.74.

Extended Data Figure 8: The fossil faunal teeth from Lida Ajer sampled for U-series dating. **a**, 7/LA/5/08 a molar of Siamang gibbon sp., sampled during our excavations. **b**, Sample 12/LA/5/08 a premolar of *Pongo* sp., sampled during our excavations. **c**, 13/LA/5/08 a molar of *Pongo* sp., sampled during our excavations. **d**, Dubois 9967A a *Pongo* sp. molar from Dubois's original excavation – kindly borrowed from Naturalis Museum in the Netherlands. **e-h**, U-series profiling tracks on the 4 fossil teeth (7,12,13, and 21/LA/5/08). **i**, Example of the best fit D-A date profile for sample 13/LA/5/08 (with 4/8=1.066 t'=1.0) demonstrating that the age estimate fits the model at ~55 kyr. The possibility of delayed uptake of uranium and the absence of evidence for uranium leaching means that this should be treated as a minimum age. The U-series profiles from other teeth did not fit well with the predictions of the D-A model due to complex U-uptake (and potentially U-loss) processes in the sampled teeth.

Extended Data Figure 9: ESR dating of two Fossil Pongo teeth 12/LA/5/08 (orange) and 13/LA/5/08 (blue). **a**, ESR dose equivalent (D_e) calculation: (Top) MCMC fitted Dose Reponses Curve (DRC) for each samples, using McDoseE 2.0 with SSE function and 100,000 iterations; (bottom) ESR dose equivalent distribution from the MCMC with McDoseE 2.0. **b**, Uranium uptake model in the different tissues used for the US/ESR age calculation. **c**, Table summarizing the U-series values (averaged) obtained by LA-MC-ICPMS on the ESR fragment and dentine directly in contact (EDJ) and used in the coupled US/ESR age model. No ages were calculated for U concentration <1ppm or U/Th ratio <500. **d**, Sample 13/LA/5/08. **e**, Sample 12/LA/5/08.

Extended Data Figure 10: Lida Ajer fossil chamber; new modelled chronology. **a**, Photograph of the fossil chamber demonstrating the location and structure of the breccia and flowstone units. **b**, Annotated photograph of the fossil chamber with the sampling locations and dating results found in Supplementary Tables 7, 8, 11. **c,** Bayesian analysis of the red TL, U-series and coupled US/ESR dating results to construct the new Lida Ajer modelled chronology. The photograph on the left (taken from dashed box in **a**) depicts the boundaries between the underlying flowstone, the breccia deposit and overlying flowstone units. Note: the red TL and ESR error on the age estimates are presented at 1σ, while the U-series errors have been presented at 2 σ. Main figure uses all the available data, while A - uses only the breccia data (from the red TL and pIR-IRSL dating of the breccia matrix and U-series dating of the flowstones and soda straw), B – uses only the fossil tooth data (from U-series age depth modelling and coupled US/ESR dating of the teeth directly).

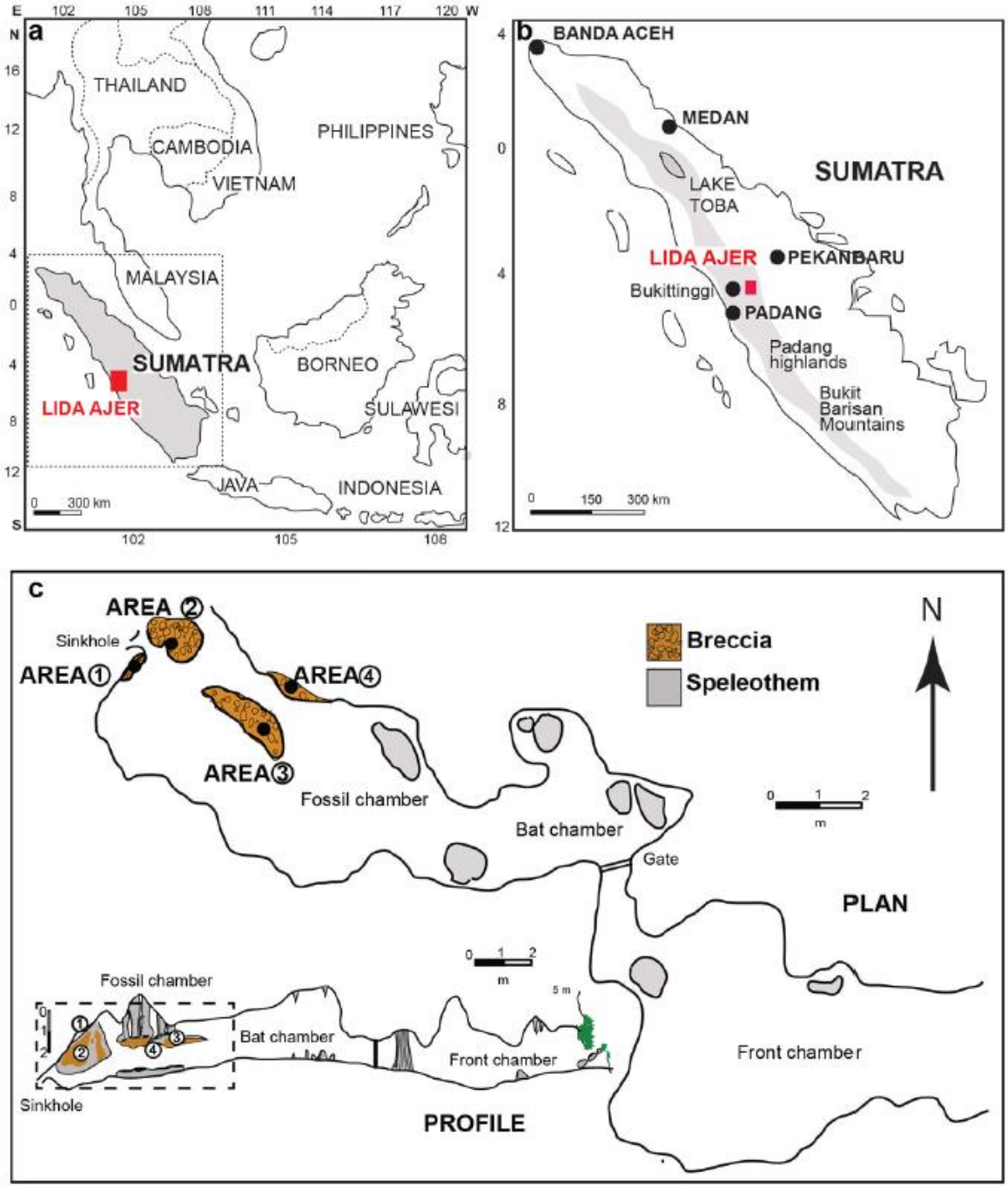
a
THAILAND
CAMBODIA
VIETNAM
PHILIPPINES
MALAYSIA
SUMATRA
LIDA AJER
BORNEO
SULAWESI
JAVA
INDONESIA
0 300 km
b
BANDA ACEH
MEDAN
SUMATRA
LAKE TOBA
LIDA AJER
PEKANBARU
Bukittinggi
PADANG
Padang highlands
Bukit Barisan Mountains
0 150 300 km
c
AREA ②
Sinkhole
AREA①
AREA④
AREA③
Fossil chamber
Bat chamber
Gate
Breccia
Speleothem
N
0 1 2 m
PLAN
Fossil chamber
Bat chamber
Front chamber
5 m
Front chamber
Sinkhole
PROFILE

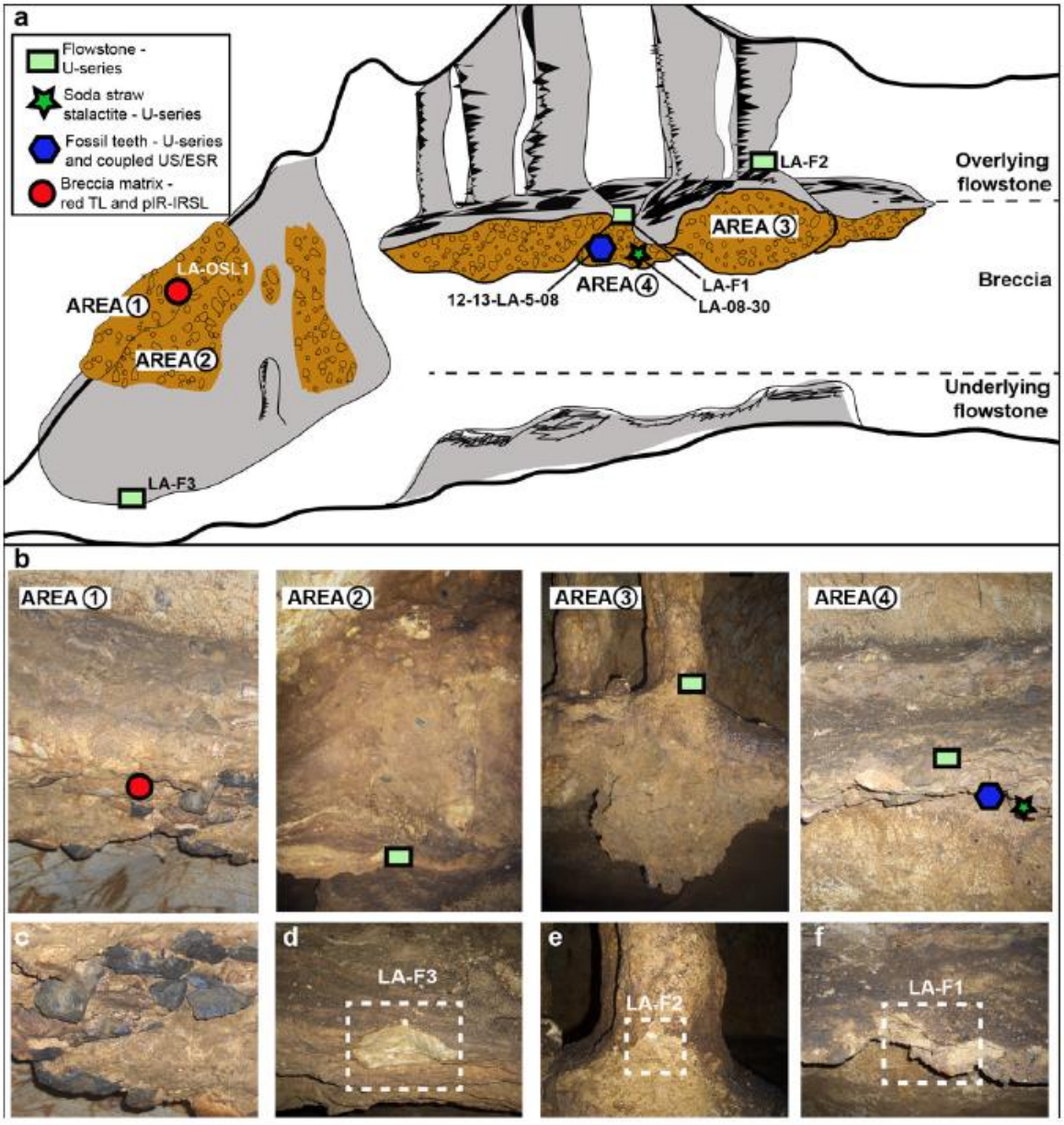
a
Flowstone - U-series
Soda straw stalactite - U-series
Fossil teeth - U-series and coupled US/ESR
Breccia matrix - red TL and pIR-IRSL
LA-F2
Overlying flowstone
AREA ③
LA-OSL1
AREA ①
AREA ④
LA-F1
LA-08-30
12-13-LA-5-08
Breccia
AREA ②
Underlying flowstone
LA-F3
b
AREA ①
AREA ②
AREA ③
AREA ④
c
d
LA-F3
e
LA-F2
f
LA-F1

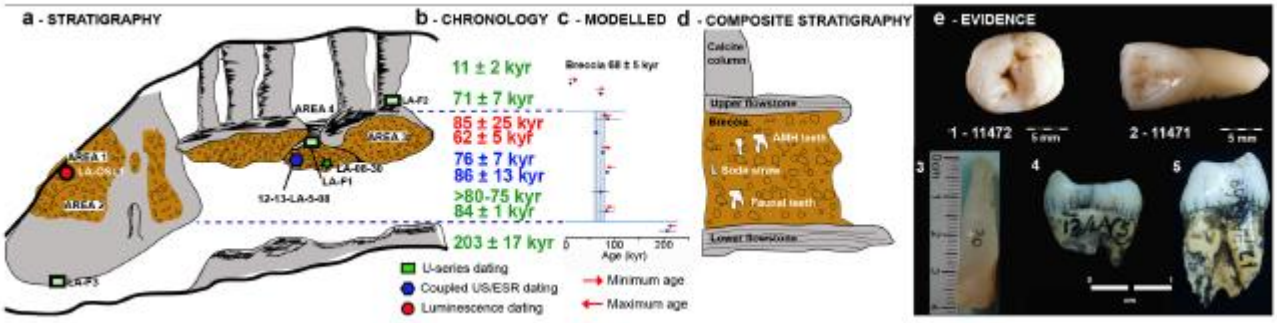
a - STRATIGRAPHY
b - CHRONOLOGY
c - MODELLED
d - COMPOSITE STRATIGRAPHY
e - EVIDENCE
11 ± 2 kyr
71 ± 7 kyr
85 ± 25 kyr
62 ± 5 kyr
76 ± 7 kyr
86 ± 13 kyr
>80-75 kyr
84 ± 1 kyr
203 ± 17 kyr
Breccia 68 ± 5 kyr
Age (kyr)
U-series dating
Coupled US/ESR dating
Luminescence dating
Minimum age
Maximum age
Calcite column
Upper flowstone
Breccia
ABH teeth
L. Soda straw
Faunal teeth
Lower flowstone
1 - 11472
2 - 11471
5 mm

Technique[a]	Sample depth (m)	Field gamma dose rate (Gy kyr^{-1})[b]	Beta dose rate (Gy kyr^{-1})[b]	Cosmic-ray dose rate (Gy kyr^{-1})[c]	Internal dose rate (Gy kyr^{-1})	Water content (%)[d]	Total dose rate (Gy kyr^{-1})[e]	Equivalent dose (Gy)[f]	Age (kyr)[g]
Red TL U	2.23	0.189 ± 0.005	0.727 ± 0.037	0.088 ± 0.009	0.030 ± 0.010	16 / 15 ± 5	1.034 ± 0.068	132 ± 13	128 ± 16
Red TL B								88 ± 25	85 ± 25
pIR-IRSL		0.189 ± 0.005	0.727 ± 0.037	0.088 ± 0.009	0.720 ± 0.020	16 / 15 ± 5	1.723 ± 0.070	105 ± 6	62 ± 5
HRGS	^{238}U (Bq/kg)	^{226}Ra (Bq/kg)	^{210}Pb (Bq/kg)	^{228}Ra (Bq/kg)	^{228}Th (Bq/kg)	^{40}K (Bq/kg)	1.141 ± 0.084		
	23 ± 3	14 ± 1	12 ± 4	19 ± 2	21 ± 7	177 ± 12			